First-principles exploration of superconductivity in MXenes

Journal:	*Nanoscale*
Manuscript ID	NR-ART-05-2020-003875.R1
Article Type:	Paper
Date Submitted by the Author:	28-Jul-2020
Complete List of Authors:	Bekaert, Jonas; University of Antwerp, Physics Sevik, Cem; Eskisehir Technical University Milosevic, Milorad; University of Antwerp, Physics

SCHOLARONE™
Manuscripts

Journal Name

First-principles exploration of superconductivity in MXenes[†]

Jonas Bekaert,[a,*,‡] Cem Sevik,[b,‡] and Milorad V. Milošević[a,§]

MXenes are an emerging class of two-dimensional materials, which in their thinnest limit consist of a monolayer of carbon or nitrogen (X) sandwiched between two transition metal (M) layers. We have systematically searched for superconductivity among MXenes for a range of transition metal elements, based on a full first-principles characterization in combination with the Eliashberg formalism. Thus, we identified six superconducting MXenes: three carbides (Mo_2C, W_2C and Sc_2C) and three nitrides (Mo_2N, W_2N and Ta_2N). The highest critical temperature of ~ 16 K is found in Mo_2N, for which a successful synthesis method has been established [Urbankowski *et al.*, Nanoscale, 2017, **9**, 17722–17730]. Moreover, W_2N presents a novel case of competing superconducting and charge density wave phases.

1 Introduction

Being one of the most recent additions to the family of two-dimensional (2D) materials[1–3], MXenes – M being a transition metal element and X either carbon or nitrogen – exhibit very versatile electronic properties, stemming from the interplay of charge, orbital and spin degrees of freedom[4–7]. Interestingly, MXenes of stoichiometry M_2X are isostructural with the 1T-phase of the transition metal dichalcogenide (TMD) family, as shown in Fig. 1. This structure is characterized by octahedral coordination of the atoms forming the central plane of the sandwich structure. Since this structure has full spatial inversion symmetry, spin-orbit coupling (SOC) does not result in spin-splitting of the bands, in contrast with, e.g., 1H-TMD monolayers which lack spatial inversion symmetry, leading to Ising-type spin-valley locking, with unconventional superconducting properties[8–11]. Nevertheless, SOC can lead to significant changes in the band structures of MXenes, especially if the transition metal element has a high atomic number, as shown in this article.

The 1T-phase of TMDs is known to host a plethora of collective quantum states, such as charge density waves (CDW) and superconductivity, both resulting from prominent electron-phonon in-

teraction in this material class[12]. Several types of CDW phases subsequently occur in 1T-TMDs as a function of temperature, finally leading to a commensurate CDW (with $\sqrt{13}a \times \sqrt{13}a$ periodicity) in the lower temperature range, accompanied by a Mott transition to an insulating state[13–17]. Hence, the CDW and superconducting phases are highly correlated, and most commonly superconductivity emerges only when the charge density wave and the corresponding periodic lattice distortion are suppressed, e.g. by pressure[16], gating[18] or doping in the van der Waals gap[19]. Moreover, dimensionality plays a key role in the behavior of these collective quantum states in 1T-TMDs. When approaching the 2D limit some compounds show weakening of the CDW state (e.g. Ta(S/Se)$_2$)[20–22], and lowering of the associated critical temperature, while others surprisingly show an enhancement (e.g. TiSe$_2$)[23] or even non-monotonic behavior as a function of the number of layers (e.g. VSe$_2$)[24].

Major differences between 1T-TMDs and MXenes arise because of the swapped positions of the transition metal atoms, forming the outer layers of the sandwich in the case of the MXenes (see Fig. 1). This also leads to very different surface properties and chemical functionalization routes[4,5,7,25–27]. Moreover, the MXene family spans a very large range of compounds, comprising transition metals of groups 3–6 of the periodic table (each of which can host different physical behavior, as e.g. discussed for CDWs in TMDs in the preceding paragraph), as well as either C or N, which have different valence[4,5,7].

While superconductivity is readily obtained in bulk-like transition metal carbides – not comprising van der Waals gaps – such as α-Mo$_2$C (with T_c of 3 K)[28–31], superconductivity in MXenes remains a largely unexplored terrain. Since the entire family of pristine MXenes is metallic[5], all possible compounds could *a priori*

a *Department of Physics & NANOlab Center of Excellence, University of Antwerp, Groenenborgerlaan 171, B-2020 Antwerp, Belgium*

b *Department of Mechanical Engineering, Faculty of Engineering, Eskisehir Technical University, 26555 Eskisehir, Turkey*

* jonas.bekaert@uantwerpen.be

§ milorad.milosevic@uantwerpen.be
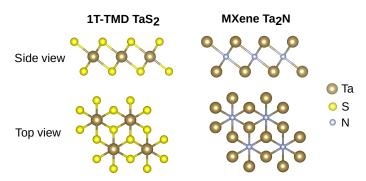
‡These authors contributed equally to this work.

Fig. 1 Comparison of the crystal structures of monolayer TaS_2 (1T-TMD) and monolayer Ta_2N (MXene).

host collective electron states like superconductivity and CDWs. Previous theoretical studies have already established monolayer Mo_2C as an electron-phonon-mediated superconductor with a critical temperature of about 6 K[32], but other compounds, especially nitrides, have remained unexplored to date.

2 Methodology

To explore new collective quantum states among MXenes we have elaborated a computational strategy to accurately scan the properties of a large variety of MXene compounds. We have considered early transition metal elements most commonly found in MXenes[1-3], namely those of groups $3-6$ (M = Sc, Ti, Zr, Hf, V, Nb, Ta, Cr, Mo, W), in combination with X = C, N, giving rise to a total of 20 compounds. These are modelled through density functional theory (DFT), as implemented within ABINIT[33], using the Perdew-Burke-Ernzerhof (PBE) functional. Using the relativistic Hartwigsen-Goedecker-Hutter (HGH) pseudopotentials[34] we could include spin-orbit coupling (SOC) where necessary. Namely, we calculated electronic structures both without and with SOC for all compounds, and if significant differences were found in the states responsible for collective electron behavior, i.e. those near the Fermi level (E_F), we proceeded with inclusion of SOC in further calculations. Within the HGH pseudopotentials $8 + N$ valence electrons for transition metal elements of group N and 4 (5) valence electrons for C (N) were taken into account. To achieve high accuracies an energy cutoff of 70 Ha for the plane-wave basis, a dense $32 \times 32 \times 1$ **k**-point grid, and at least 16 Å of vacuum in the unit cell were used, and the crystal structures were relaxed so forces on each atom were below 1 meV/Å. To further characterize the MXene Fermi surfaces we have calculated Fermi velocities from the electronic band structures by $\mathbf{v}_F = \hbar^{-1} \nabla_{\mathbf{k}} \varepsilon_{\mathbf{k}} |_{\varepsilon = E_F}$.

Subsequently, to calculate phonons and electron-phonon coupling we have employed density functional perturbation theory (DFPT)[35], also within ABINIT, using $32 \times 32 \times 1$ electronic **k**-point grids and $16 \times 16 \times 1$ phononic **q**-point grids. Here, we have investigated the dynamical stabilities of the crystal structures with respect to the electronic occupation numbers used within our DFPT calculations. Namely, it is well known from *ab initio* research on CDW behavior in TMDs that one can resolve such structural phase transitions at reduced temperatures using sufficiently small thermal broadening[36]. In this case, phonon soft-

ening and emerging unstable phonon modes are found, whose phonon wave vectors indicate the preferred crystal reconstruction. Hence, we have compared results obtained with relatively high (0.01 Ha) and low (0.0025 Ha) broadening factors of the Fermi-Dirac smearing function for electronic occupations to identify new CDW-type instabilities in MXenes. For the superconducting state we have used Eliashberg theory, a quantitatively accurate extension to the Bardeen-Cooper-Schrieffer (BCS) theory for phonon-mediated superconductivity[37-39]. Using the density of states at the Fermi level (N_F), the matrix elements of the electron-phonon coupling ($g_{\mathbf{k,k+q}}^v$), and the phonon ($\omega_{\mathbf{q}}^v$) and electron ($\varepsilon_{\mathbf{k}}$) band structures (with E_F at 0) obtained from our *ab initio* calculations, we have evaluated Eliashberg functions,

$$\alpha^2 F(\omega) = \frac{1}{N_F} \sum_{v,\mathbf{k},\mathbf{q}} \left| g_{\mathbf{k,k+q}}^v \right|^2 \delta\left(\omega - \omega_{\mathbf{q}}^v\right) \delta\left(\varepsilon_{\mathbf{k}}\right) \delta\left(\varepsilon_{\mathbf{k+q}}\right) , \quad (1)$$

of the different MXenes, and the corresponding electron-phonon coupling (EPC) constants by $\lambda = 2 \int_0^\infty \alpha^2 F(\omega) \omega^{-1} d\omega$. Based on these results we have subsequently evaluated the superconducting T_c using the Allen-Dynes formula[40-42], and a screened Coulomb repulsion of $\mu^* = 0.13$ – a standard value for transition metal-based compounds[43]. If the EPC is too weak for Cooper-pair formation, this formula yields $T_c \approx 0$, indicating the compound is non-superconducting.

3 Results

A complete overview of the obtained results is provided in Table 1. Superconductivity is thus found in Mo and W carbides and nitrides (where the nitrides exhibit the higher T_c in both cases), as well as in Ta_2N and Sc_2C. The complete set of data – electronic band structures and density of states, Fermi surfaces together with Fermi velocities, phonon band structures and phonon density of states, Eliashberg functions and electron-phonon coupling constants – is presented in the Supplemental Information[†]. In what follows we set out to explain these results.

Considering first MXenes composed of transition metal elements of group 6 of the periodic system (Cr, Mo, W), we found them to be the most promising ones for superconductivity, at least in the case of Mo and W. The band structures of these carbides and nitrides, shown in Fig. 2a–d, show changes due to SOC to be negligible in the case of Mo (in combination with both C or N), but fairly strong for W, the heaviest element to be found in MXenes ($Z = 74$). The resulting Fermi surface of Mo_2C, shown in Fig. 2e, consists of three distinctly different sheets: (i) six small electron-like pockets around Γ, (ii) a larger circular electron-like sheet also centered around Γ, and (iii) an oval sheet centered around M, the latter two nearly touching along $\Gamma - M$. In comparison, in the case of Mo_2N (Fig. 2f) a fourth sheet appears at E_F, shaped as a six-bladed propeller around Γ, however, the pocket around M is markedly reduced in size. The band structure of W_2C (Fig. 2c) features a rather flat section along $\Gamma - K$, leading to the ship's wheel-like shape of the Fermi sheet centered around Γ, as shown in Fig. 2g. The Fermi surface of W_2N, shown in Fig. 2h, consists of two nested six-bladed propellers around Γ, thus, it is lacking the hole-like pocket around M, found in all the other

MXene	SOC included (*yes/no*)	a (Å)	N_F (eV^{-1})	v_F (10^6 m/s)	T_c (K)	$\xi(0)$ (nm)
Mo$_2$C	y	3.001	3.08	0.258	5.8	45
Mo$_2$C	n	3.001	3.19	0.260	7.1	37
Mo$_2$N	y	2.811	2.32	0.341	15.5	22
Mo$_2$N	n	2.807	2.58	0.343	16.0	20
W$_2$C	y	2.869	1.84	0.257	5.8	45
W$_2$C	n	2.865	3.06	0.317	4.2	77
W$_2$N	y	2.779	1.72	0.359	9.7	38
W$_2$N	n	2.773	1.96	0.349	9.8	36
Ta$_2$N	y	3.078	1.36	0.451	2.4	191
Ta$_2$N	n	3.089	1.40	0.454	2.1	220
Sc$_2$C	y	3.320	4.10	0.140	4.0	36
Sc$_2$C	n	3.320	4.10	0.140	4.1	35
Cr$_2$C*	y	2.806	4.82	0.165	-	-
Cr$_2$N	y	2.662	2.45	0.205	-	-
V$_2$C	n	2.899	3.27	0.142	-	-
V$_2$N	n	2.897	1.61	0.297	-	-
Nb$_2$C	y	3.121	2.94	0.281	-	-
Nb$_2$N	y	3.138	1.35	0.406	-	-
Ta$_2$C	y	3.073	2.00	0.281	-	-
Ti$_2$C	n	3.037	4.51	0.219	-	-
Ti$_2$N	n	2.980	5.50	0.175	-	-
Zr$_2$C	n	3.267	3.37	0.319	-	-
Zr$_2$N	n	3.240	3.41	0.256	-	-
Hf$_2$C	n	3.205	3.21	0.317	-	-
Hf$_2$N	n	3.167	3.14	0.284	-	-
Sc$_2$N	n	3.188	3.47	0.227	-	-

Table 1 Calculated lattice constant (a), electronic DOS at the Fermi level (N_F), average Fermi velocity (v_F), superconducting transition temperature (T_c) and coherence length at $T = 0$ ($\xi(0)$) for all considered MXenes. *Dynamically unstable.

compounds. Overall, MXene Fermi surfaces display a wealth of different shapes and configurations, in contrast to those of 1T-TMD monolayers (in the non-CDW state), which typically consist of a single sheet centered around M [44,45]. Our complete set of calculated Fermi surfaces, including Fermi velocities, can be found in the Supplementary Information[†].

Phonon dispersions of these four compounds and the corresponding phonon DOS, calculated using DFPT, are shown in Fig. 3. Whereas the carbides have a clear gap between Mo/W-based modes and C modes, in the nitrides the N-based modes display a remarkably strong dispersion (this also holds true for Cr$_2$N, see Supplementary Information[†]), which strongly reduces the phonon energy gap, even closing it in the case of Mo$_2$N. As a result, the Eliashberg function of Mo$_2$C features separate Mo and C domes (Fig. 4a), whereas a continuous spectrum is found in the case of Mo$_2$N (Fig. 4b). In spite of its slightly lower DOS (see Table 1), the overall stronger EPC in Mo$_2$N ($\lambda = 1.2$) compared to Mo$_2$C ($\lambda = 0.75$) yields a three times higher T_c for the former, 15.5 K vs. 5.8 K. This stronger EPC in Mo$_2$N stems from two sources. Firstly, the Eliashberg function of Mo$_2$N features three strong peaks within the Mo-based modes – indicated by I-III in Fig. 4(b) – in contrast to only two peaks in the case of Mo$_2$C (Fig. 4(a)). Namely, coupling to the flexural mode (mode I, shown in Fig. 4(e)) is strong in Mo$_2$N, while no clear peak related to this mode is present in Mo$_2$C. The other two main peaks in their Eliashberg functions stem from in-plane (II) and out-of-plane (III) optical Mo-based modes (depicted in Fig. 4(e)). Secondly, the N-

based modes in Mo$_2$N are softer, and show much stronger dispersion, than the corresponding C-based modes in Mo$_2$C (cf. Fig. 3 (a) and (b)), thus the N-modes contribute more to $\alpha^2 F(\omega)\omega^{-1}$, yielding a higher λ. Therefore, Mo$_2$N possesses the highest T_c of all investigated MXenes. Moreover, Mo$_2$N is one of the few nitride MXenes that has already been synthesized, by means of an ammoniation process [46], facilitating experimental confirmation of its predicted superconducting properties.

The Eliashberg function of W$_2$C (Fig. 4c) is similar to the one of Mo$_2$C, resulting in a similar T_c of 5.8 K. On the other hand, the phonon band structure of W$_2$N (Fig. 3d) stands out, as it develops a partially unstable W-based acoustic mode at reduced smearing (imaginary phonon frequencies, here mapped to negative real numbers), centered around M. Such evanescent phonon mode in a limited portion of the Brillouin zone corresponds to a CDW instability, here described by wavenumber $q_{CDW} = M = \frac{a^*}{2}$, where a^* is the magnitude of the reciprocal lattice vectors. The commensurability relation between the CDW and the reciprocal lattice vectors, $n \cdot q_{CDW} = m \cdot a^*$ (with n and m relative prime numbers), is therefore fulfilled by $(n, m) = (2, 1)$. The wave length of the CDW is thus $\lambda_{CDW} = 2a$. Taking into account in-plane rotation symmetry, the CDW-driven periodic lattice distortion (PLD) adopts a commensurate $2 \times 2 \times 1$ supercell of the original lattice. When discarding the contribution of the unstable modes, as shown in Fig. 4d, significant EPC of $\lambda = 1.1$ is obtained (with inclusion of SOC), resulting in $T_c = 9.7$ K. However, the PLD would alter the electronic structure (usually partial gapping of the Fermi sur-
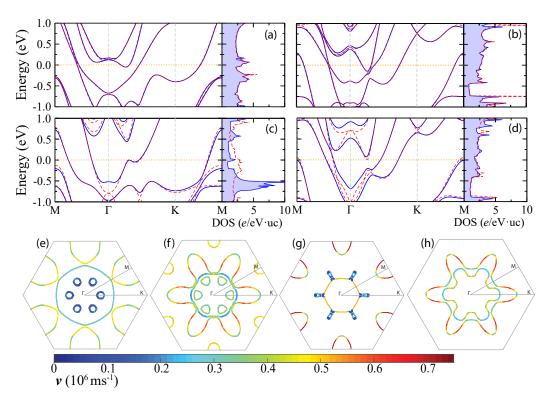
Fig. 2 Band structure and Fermi surface (colored according to the Fermi velocities) for (a),(e) Mo$_2$C, (b),(f) Mo$_2$N, (c),(g) W$_2$C, and (d),(h) W$_2$N. Blue solid lines and red dashed lines show the results calculated with and without spin-orbit coupling, respectively.
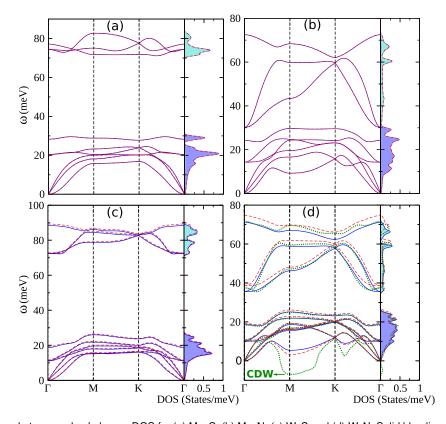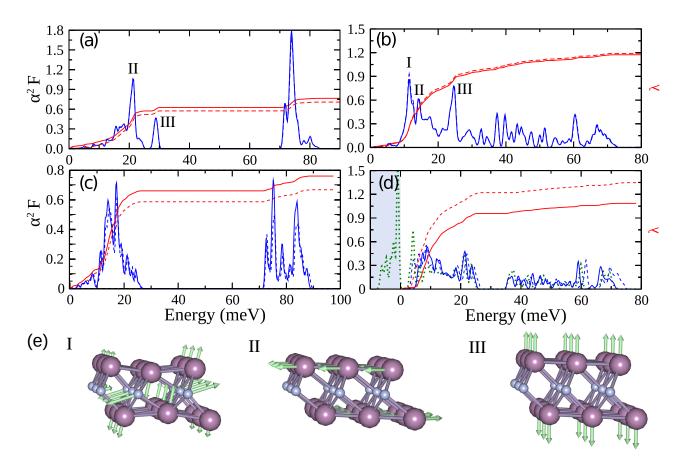

Fig. 3 Phonon dispersion and atom-resolved phonon DOS for (a) Mo$_2$C, (b) Mo$_2$N, (c) W$_2$C and (d) W$_2$N. Solid blue lines and red dashed lines show the results calculated with and without spin-orbit coupling, respectively. Cyan and violet areas show the contributions from C/N and Mo/W to the phonon DOS, respectively. Green dotted lines show the results obtained with lower electronic smearing for W$_2$N (d).
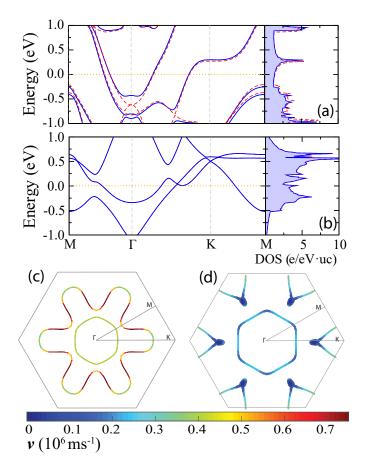
Fig. 4 Eliashberg function (blue) and EPC λ (red) for (a) Mo_2C, (b) Mo_2N, (c) W_2C and (d) W_2N. Solid and dashed lines show the results calculated with and without spin-orbit coupling, respectively. The green dotted line shows the result obtained with lower electronic smearing for W_2N (d). (e) Phonon modes corresponding to peaks in the Eliashberg functions, shown in (a) and (b).

face) and the electron-phonon interaction, so intricate interplay between the CDW and superconductivity phases is expected[47]. Such interplay has to date only been found in TMDs (T and H polytypes), where the CDW originates from the inner transition metal layer of the structure. In W_2N, on the other hand, the CDW is driven by phonon modes stemming from W, hence the PLD mainly occurs in the outer layers of the structure, where W is located. This likely makes the CDW state in W_2N more prone to tuning by controlled surface functionalization.

Among MXenes containing group 6 transition metal elements, Cr-based compounds are a special case. While Cr_2N simply exhibits very low coupling of electrons to any phonon mode, Cr_2C hosts various instabilities. These originate from its flat electronic dispersion around Γ right at E_F, and the corresponding peak in the density of states (DOS), as shown in the Supplementary Information[†]. This introduces a ferromagnetic instability in Cr_2C, according to the Stoner criterion. As a result of the inclusion of SOC in our calculations we even found the paramagnetic state of Cr_2C to feature an evanescent phonon mode throughout the entire Brillouin zone, indicating dynamical instability. Nevertheless, we found that the peak in the DOS can be removed by applying compressive strain (-4% was sufficient) to suppress the ferromagnetic state. Since our calculations indicate Cr_2C to host sizeable electron-phonon coupling (see Supplementary Information[†]), it is a good candidate for strain-tunable in-

terplay between phonon-mediated superconductivity and concurrent spin fluctuations, stemming from the competing magnetic state. Such a system is promising for unconventional, e.g. triplet pairing-based, superconductivity, which can be explored using recent advances in *ab initio* methods[48].

Only one new superconducting compound was found among MXenes based on group 5 transition metal elements (V, Nb, Ta), namely Ta_2N, whose band structure is depicted in Fig. 5a. Although the inclusion of SOC leads to significant changes below E_F, the Fermi surface itself is hardly affected. It is moreover very similar for all M_2N compounds (where M is a group 5 element), consisting of a circular sheet inside a six-bladed propeller (see Fig. 5c). However, the higher mass of Ta leads to a phonon redshift compared to the other compounds (see Fig. 6a,c and the Supplementary Information[†]), boosting the EPC in Ta_2N to $\lambda = 0.6$ (also much higher than its carbide counterpart, Ta_2C, with $\lambda = 0.1$, see Supplementary Information[†]), yielding $T_c = 2.4$ K. However, by applying in-plane tensile strain the phonons of compounds with analogous Eliashberg functions, like Nb_2C and Nb_2N, can be redshifted to enhance the EPC and thus induce superconductivity[49,50]. Similarly, the T_c of Ta_2N can likely be enhanced by tensile strain. Our result on the absence of intrinsic superconductivity in Nb_2C has been confirmed by recent transport measurements[51]. Nevertheless, it was found that superconductivity can be induced in Nb_2C by surface functionalization[51,52],

Fig. 5 Band structure and Fermi surface (including Fermi velocities) for Ta$_2$N [(a),(c)], and Sc$_2$C [(b),(d)]. Solid blue lines and red dashed lines show the results calculated with and without spin-orbit coupling, respectively.

leading to T_c's up to 6 K in case of Cl and S surface terminations and reaching up to 7 K in case of the NH functional group[51]. The emergence of superconductivity was shown to be correlated with in-plane lattice expansions due to functionalization[51], in agreement with our prediction of enhanced electron-phonon coupling due to tensile strain.

Group 4 of the periodic system (Ti, Zr, Hf) is the only one not hosting new superconducting MXenes. All compounds based on these elements were found to have low EPC within the range $0.2 - 0.3$, in spite of their high DOS at E_F (see Table 1 and the Supplementary Information[†]). Finally, group 3 with the lightest transition metal, Sc ($Z = 21$), contributes a sixth new superconducting compound, namely Sc$_2$C. Its band structure, shown in Fig. 5b, features a crossing point along $\Gamma - K$ at $\sim$30 meV above E_F. We note that other investigated – yet non-superconducting – MXenes host similar crossing points in the vicinity of E_F, e.g. (V,Nb,Ta)$_2$C and (Ti,Zr,Hf)$_2$N (see Supplementary Information[†]). The rather unconventional band dispersion of Sc$_2$C results in a mini-pocket attached to the larger Fermi sheet centered around K, as shown in Fig. 5d. Sc$_2$C hosts moderate EPC, with $\lambda = 0.6$ (see Fig. 6d), yielding $T_c = 4$ K. Since the crossing point lies well within the energy window around E_F where superconductivity develops – as dictated by the phonon frequencies of Sc$_2$C, reach-

ing values up to 70 meV (see Fig. 6b) – it may introduce unconventional properties in the superconducting state, in view of the linear dispersion of some of the band segments.

Based on our calculations we can also predict the coherence length of the different superconducting MXenes, i.e. the characteristic healing length of the superconducting order parameter around perturbations like defects or penetrating magnetic field and vortices, via the microscopic Ginzburg-Landau relation $\xi(0) = \sqrt{\frac{7\zeta(3)}{3}} \frac{\hbar v_F}{4\pi T_c}$ [53], where v_F is the average Fermi velocity. The results, listed in Table 1, highlight the diverse superconducting properties of MXenes, with values of coherence lengths ranging from 22 nm (in Mo$_2$N) to 191 nm (in Ta$_2$N).

4 Conclusions

We have performed a first-principles exploration of new superconductors among monolayer MXenes, considering all combinations of ten transition metal elements from groups 3–6 of the periodic system with C and N. To assess potential superconductivity we have used the Eliashberg formalism combined with *ab initio* calculated electronic and vibrational properties, as well as the electron-phonon interaction. Our search has yielded six new monolayer superconductors: Group 6 has proven particularly fruitful, as all Mo- and W-based MXenes are superconducting. Their T_c's range from 6 K in Mo$_2$C to 16 K in Mo$_2$N, a compound for which a successful synthesis method is available[46]. Furthermore, one additional superconducting compound was found among group 5-based MXenes, namely Ta$_2$N with T_c of 2 K, and one among group 3-based MXenes, Sc$_2$C with T_c of 4 K.

Moreover, in our search we identified other interesting quantum states that coexist or compete with superconductivity – such as magnetism in Cr$_2$C – resulting from the rich interplay between charge, orbital, spin and structural degrees of freedom in MXenes. We identified W$_2$N as a novel charge density wave (CDW) material, based on a commensurate phonon instability for λ_{CDW} equal to twice the lattice parameter (see Fig. 3d). The corresponding 2×2 in-plane periodically distorted W$_2$N lattice, in combination with strong electron-phonon interaction, provides a very rare non-TMD system where the interplay between CDW and superconducting states can be explored. We therefore conclude that MXenes represent an exciting new class of ultrathin superconductors, with multi-functional properties and interplay of quantum phenomena worthy of further exploration.

Conflicts of interest

There are no conflicts to declare.
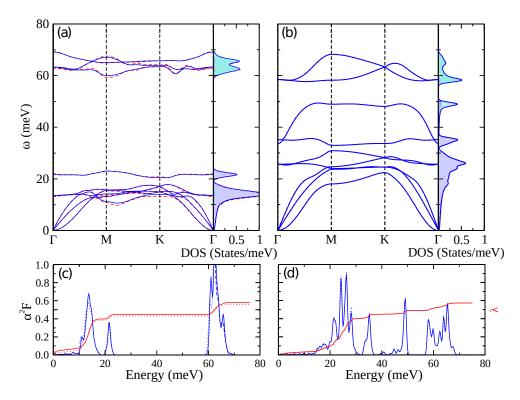
Acknowledgements

Fig. 6 Phonon dispersion and atom-resolved phonon DOS for (a) Ta$_2$N, and (b) Sc$_2$C. Here, solid blue lines and red dashed lines show the results calculated with and without spin-orbit coupling, respectively. Cyan and violet areas show the contributions from N/C and Ta/Sc to the phonon DOS, respectively. Isotropic Eliashberg function (blue) and EPC λ (red) for (a) Ta$_2$N, and (b) Sc$_2$C. Here, solid lines and dashed lines show the results calculated with and without spin-orbit coupling, respectively.

Notes and references

1 M. Naguib, M. Kurtoglu, V. Presser, J. Lu, J. Niu, M. Heon, L. Hultman, Y. Gogotsi and M. W. Barsoum, *Adv. Mater.*, 2011, **23**, 4248–4253.

2 M. Naguib, O. Mashtalir, J. Carle, V. Presser, J. Lu, L. Hultman, Y. Gogotsi and M. W. Barsoum, *ACS Nano*, 2012, **6**, 1322–1331.

3 M. Naguib, J. Halim, J. Lu, K. M. Cook, L. Hultman, Y. Gogotsi and M. W. Barsoum, *J. Am. Chem. Soc.*, 2013, **135**, 15966–15969.

4 M. Naguib, V. N. Mochalin, M. W. Barsoum and Y. Gogotsi, *Adv. Mater.*, 2014, **26**, 992–1005.

5 M. Khazaei, A. Ranjbar, M. Arai, T. Sasaki and S. Yunoki, *J. Mater. Chem. C*, 2017, **5**, 2488–2503.

6 B. Anasori, M. R. Lukatskaya and Y. Gogotsi, *Nat. Rev. Mater.*, 2017, **2**, 16098.

7 Y. Gogotsi and B. Anasori, *ACS Nano*, 2019, **13**, 8491–8494.

8 J. M. Lu, O. Zheliuk, I. Leermakers, N. F. Q. Yuan, U. Zeitler, K. T. Law and J. T. Ye, *Science*, 2015, **350**, 1353–1357.

9 Y. Saito, Y. Nakamura, M. S. Bahramy, Y. Kohama, J. Ye, Y. Kasahara, Y. Nakagawa, M. Onga, M. Tokunaga, T. Nojima, Y. Yanase and Y. Iwasa, *Nat. Phys.*, 2015, **12**, 144.

10 X. Xi, Z. Wang, W. Zhao, J.-H. Park, K. T. Law, H. Berger, L. Forro, J. Shan and K. F. Mak, *Nat. Phys.*, 2016, **12**, 139–143.

11 Y. Xing, K. Zhao, P. Shan, F. Zheng, Y. Zhang, H. Fu, Y. Liu, M. Tian, C. Xi, H. Liu, J. Feng, X. Lin, S. Ji, X. Chen, Q.-K. Xue and J. Wang, *Nano Lett.*, 2017, **17**, 6802–6807.

12 S. Manzeli, D. Ovchinnikov, D. Pasquier, O. V. Yazyev and A. Kis, *Nat. Rev. Mater.*, 2017, **2**, 17033.

13 A. J. Wilson, J. F. D. Salvo and S. Mahajan, *Adv. Phys.*, 1975, **24**, 117.

14 C. B. Scruby, P. M. Williams and G. S. Parry, *Philosophical Magazine*, 1975, **31**, 255.

15 E. R. Thomson, B. Burk, A. Zettl and J. Clarke, *Phys. Rev. B*, 1994, **49**, 16899.

16 B. Sipos, A. F. Kusmartseva, A. Akrap, H. Berger, L. Forró and E. Tutis, *Nat. Mater.*, 2008, **7**, 960–965.

17 T. Ritschel, J. Trinckauf, K. Koepernik, B. Büchner, M. v. Zimmermann, H. Berger, Y. I. Joe, P. Abbamonte and J. Geck, *Nat. Phys.*, 2015, **11**, 328.

18 L. J. Li, E. C. T. O'Farrell, K. P. Loh, G. Eda, B. Özyilmaz and A. H. Castro Neto, *Nature*, 2015, **529**, 185.

19 E. Morosan, H. W. Zandbergen, B. S. Dennis, J. W. G. Bos, Y. Onose, T. Klimczuk, A. P. Ramirez, N. P. Ong and R. J. Cava, *Nat. Phys.*, 2006, **2**, 544.

20 A. W. Tsen, R. Hovden, D. Wang, Y. D. Kim, J. Okamoto, K. A. Spoth, Y. Liu, W. Lu, Y. Sun, J. C. Hone, L. F. Kourkoutis,

P. Kim and A. N. Pasupathy, *Proc. Natl. Acad. Sci. U.S.A.*, 2015, **112**, 15054–15059.

21 P. C. Börner, M. K. Kinyanjui, T. Björkman, T. Lehnert, A. V. Krasheninnikov and U. Kaiser, *Appl. Phys. Lett.*, 2018, **113**, 173103.

22 R. Samnakay, D. Wickramaratne, T. R. Pope, R. K. Lake, T. T. Salguero and A. A. Balandin, *Nano Lett.*, 2015, **15**, 2965–2973.

23 S. Kolekar, M. Bonilla, Y. Ma, H. C. Diaz and M. Batzill, *2D Mater.*, 2018, **5**, 015006.

24 A. Pásztor, A. Scarfato, C. Barreteau, E. Giannini and C. Renner, *2D Mater.*, 2017, **4**, 041005.

25 M. Khazaei, M. Arai, T. Sasaki, M. Estili and Y. Sakka, *Phys. Chem. Chem. Phys.*, 2014, **16**, 7841–7849.

26 U. Yorulmaz, A. Özden, N. K. Perkgöz, F. Ay and C. Sevik, *Nanotechnology*, 2016, **27**, 335702.

27 J. L. Hart, K. Hantanasirisakul, A. C. Lang, B. Anasori, D. Pinto, Y. Pivak, J. T. van Omme, S. J. May, Y. Gogotsi and M. L. Taheri, *Nat. Commun.*, 2019, **10**, 522.

28 C. Xu, L. Wang, Z. Liu, L. Chen, J. Guo, N. Kang, X.-L. Ma, H.-M. Cheng and W. Ren, *Nat. Mater.*, 2015, **14**, 1135–1141.

29 L. Wang, C. Xu, Z. Liu, L. Chen, X. Ma, H.-M. Cheng, W. Ren and N. Kang, *ACS Nano*, 2016, **10**, 4504–4510.

30 Z. Liu, C. Xu, N. Kang, L. Wang, Y. Jiang, J. Du, Y. Liu, X.-L. Ma, H.-M. Cheng and W. Ren, *Nano Lett.*, 2016, **16**, 4243–4250.

31 D. Geng, X. Zhao, L. Li, P. Song, B. Tian, W. Liu, J. Chen, D. Shi, M. Lin, W. Zhou and K. P. Loh, *2D Mater.*, 2016, **4**, 011012.

32 J.-J. Zhang and S. Dong, *J. Chem. Phys.*, 2017, **146**, 034705.

33 X. Gonze, F. Jollet, F. A. Araujo, D. Adams, B. Amadon, T. Applencourt, C. Audouze, J.-M. Beuken, J. Bieder, A. Bokhanchuk, E. Bousquet, F. Bruneval, D. Caliste, M. Côté, F. Dahm, F. D. Pieve, M. Delaveau, M. D. Gennaro, B. Dorado, C. Espejo, G. Geneste, L. Genovese, A. Gerossier, M. Giantomassi, Y. Gillet, D. Hamann, L. He, G. Jomard, J. L. Janssen, S. L. Roux, A. Levitt, A. Lherbier, F. Liu, I. Lukačević, A. Martin, C. Martins, M. Oliveira, S. Poncé, Y. Pouillon, T. Rangel, G.-M. Rignanese, A. Romero, B. Rousseau, O. Rubel, A. Shukri, M. Stankovski, M. Torrent, M. V. Setten, B. V. Troeye,

M. Verstraete, D. Waroquiers, J. Wiktor, B. Xu, A. Zhou and J. Zwanziger, *Comput. Phys. Commun.*, 2016, **205**, 106 – 131.

34 C. Hartwigsen, S. Goedecker and J. Hutter, *Phys. Rev. B*, 1998, **58**, 3641–3662.

35 S. Y. Savrasov and D. Y. Savrasov, *Phys. Rev. B*, 1996, **54**, 16487–16501.

36 O. R. Albertini, A. Y. Liu and M. Calandra, *Phys. Rev. B*, 2017, **95**, 235121.
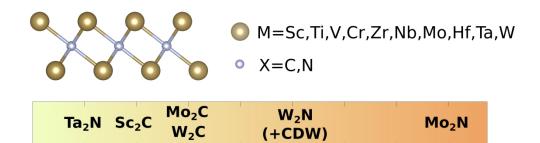
37 G. M. Eliashberg, *JETP*, 1960, **11**, 696.

38 G. M. Eliashberg, *JETP*, 1961, **12**, 1000.

39 F. Giustino, *Rev. Mod. Phys.*, 2017, **89**, 015003.

40 W. L. McMillan, *Phys. Rev.*, 1968, **167**, 331–344.

41 P. B. Allen and R. C. Dynes, *Phys. Rev. B*, 1975, **12**, 905–922.

42 P. B. Allen and B. Mitrović, *Theory of Superconducting T_c*, Academic Press, 1983, vol. 37, pp. 1 – 92.

43 G. Grimvall, *The electron-phonon interaction*, North Holland Publishing Co., 1981.

44 J.-A. Yan, M. A. D. Cruz, B. Cook and K. Varga, *Sci. Rep.*, 2015, **5**, 16646.

45 G. Duvjir, B. K. Choi, I. Jang, S. Ulstrup, S. Kang, T. Thi Ly, S. Kim, Y. H. Choi, C. Jozwiak, A. Bostwick, E. Rotenberg, J.-G. Park, R. Sankar, K.-S. Kim, J. Kim and Y. J. Chang, *Nano Lett.*, 2018, **18**, 5432–5438.

46 P. Urbankowski, B. Anasori, K. Hantanasirisakul, L. Yang, L. Zhang, B. Haines, S. J. May, S. J. L. Billinge and Y. Gogotsi, *Nanoscale*, 2017, **9**, 17722–17730.

47 F. Zheng and J. Feng, *Phys. Rev. B*, 2019, **99**, 161119.

48 J. Bekaert, A. Aperis, B. Partoens, P. M. Oppeneer and M. V. Milošević, *Phys. Rev. B*, 2018, **97**, 014503.

49 J. Bekaert, A. Aperis, B. Partoens, P. M. Oppeneer and M. V. Milošević, *Phys. Rev. B*, 2017, **96**, 094510.

50 J. Bekaert, M. Petrov, A. Aperis, P. M. Oppeneer and M. V. Milošević, *Phys. Rev. Lett.*, 2019, **123**, 077001.

51 V. Kamysbayev, A. S. Filatov, H. Hu, X. Rui, F. Lagunas, D. Wang, R. F. Klie and D. V. Talapin, *Science*, 2020.

52 Z. U. D. Babar, M. S. Anwar, M. Mumtaz, M. Iqbal, R.-K. Zheng, D. Akinwande and S. Rizwan, *2D Materials*, 2020, **7**, 035012.

53 A. L. Fetter and J. D. Walecka, *Quantum Theory of Many-Particle Systems*, Dover Publications, 2003.

New superconducting MXenes are presented, discovered through extensive first-principles exploration, furthermore hosting interplay with other quantum phases, such as charge density waves.

2139x829mm (94 x 94 DPI)